Characterization of linear viscoelastic, nonlinear viscoelastic and damage stages of asphalt mixtures[1]

Rong Luo, Ph.D., P.E.
Professor
School of Transportation
Wuhan University of Technology
1178 Heping Avenue
Wuhan, Hubei Province 430063, China
Phone: +86 (27) 8653 1551
Fax: +86 (27) 8653 1551
Email: rongluo@whut.edu.cn

Hanqi Liu, Ph.D. Candidate
Graduate Research Assistant
School of Transportation
Wuhan University of Technology
1178 Heping Avenue
Wuhan, Hubei Province 430063, China
Phone: +86 (27) 8653 1551
Fax: +86 (27) 8653 1551
Email: hanqiliu@whut.edu.cn

Yuqing Zhang, Ph.D.
Lecturer
School of Engineering and Applied Science
Aston University
MB153A, Aston Triangle
Birmingham, B4 7ET, U.K.
Phone: +44 (0) 121-204-3391
Email: y.zhang10@aston.ac.uk

---

39 **Abstract**

40   It has been demonstrated that asphalt mixtures experienced linear viscoelastic stage,

41 nonlinear viscoelastic stage and damage stage when subjected to controlled-strain repeated

42 direct-tension (RDT) tests with increasing strain levels. However, the linear viscoelastic

43 properties of asphalt mixtures are usually muddled up with their nonlinear viscoelastic

44 properties. These confusions directly lead to the incorrect determination of the pseudostrains

45 and dissipated pseudostrain energies (DPSEs) in the nonlinear viscoelastic stage and damage

46 stage. This study investigated the material properties of fine aggregate mixture (FAM)

47 specimens in all three stages. These three stages were differentiated and characterized in

48 terms of the viscoelastic stress, pseudostrain and DPSE. The definitions of viscoelastic stress,

49 reference modulus and pseudostrain were rigorously established to assure that the material

50 properties in the linear viscoelastic stage were the reference properties and that the sole linear

51 viscoelastic effect was eliminated when determining the pseudostrain and DPSE in the three

52 stages. The characteristics of the DPSE in the three stages were found to be: 1) the DPSE of

53 any loading cycle was zero in the linear viscoelastic stage; 2) in the nonlinear viscoelastic

54 stage, the DPSE of each loading cycle remained approximately the same with the growth of

55 the number of loading cycles, and the DPSE increased to a larger value when the strain level

56 of the RDT test increased to a higher level; 3) in the damage stage, the DPSE of the loading

57 cycle increased as the number of loading cycles increased. This study strictly distinguished

58 the linear viscoelasticity from the nonlinear viscoelasticity of the asphalt mixtures, which is

59 critical for the accurate determination of the DPSE spent in overcoming the nonlinear

60 viscoelasticity and in developing damages, such as cracking and permanent deformation, in

61 the asphalt mixtures.

62

63 **Keywords:**

64 Asphalt mixture; linear viscoelasticity; nonlinear viscoelasticity; viscoelastic stress;

65 pseudostrain; dissipated pseudostrain energy.

66 **1. Introduction**

67   Paving asphalt mixtures are complex composite materials that may exhibit different

68 properties at different strain levels. It has been demonstrated that, when subjected to typical

69 controlled-strain repeated direct-tension (RDT) tests, an asphalt mixture experiences multiple

70 stages as the strain level increases, which include: 1) undamaged stage, consisting of the

71 linear viscoelastic stage and the nonlinear viscoelastic stage; and 2) damage stage [1][2].

72 These stages have the following characteristics:

73   (1) Undamaged stage:

74   a. At any specific strain level, the material properties stay constant despite of

75   the increase of the number of loading cycles;

76   b. The deformation of the asphalt mixture is completely recovered after

77   unloading;

78   c. As the strain level varies, the asphalt mixture has different properties in the

79   linear viscoelastic stage from those in the nonlinear viscoelastic stage:

80   i. Linear viscoelastic stage: the material properties remain unchanged

81   if the strain level varies within this stage;

82   ii. Nonlinear viscoelastic stage: the material properties change as the

83   strain level varies;

84   (2) Damage stage:

85   a. At any specific strain level, the material properties vary with the increase

86   of the number of loading cycles;

87   b. The deformation of the asphalt mixture cannot be completely recovered

88   after unloading; and

89   c. The material properties change as the strain level varies.

90 If using the pseudostrain defined in Equation 1 to eliminate the linear viscoelastic effect [3],

91 these stages can be illustrated via the stress-pseudostrain curve, as shown in Figure 1.

92
$$\varepsilon_R = \frac{\sigma_{VE}(t)}{E_R} = \frac{\int_0^t E(t-\tau)\frac{\partial \varepsilon(\tau)}{\partial \tau}d\tau}{E_R} \tag{1}$$

93 where ε_R = pseudostrain, $\mu\varepsilon$; $\sigma_{VE}(t)$ = viscoelastic stress corresponding to the measured

94 strain history, Pa; E_R = reference modulus, MPa; t = loading time, s; τ = a dummy variable,

95 indicating any arbitrary time between 0 and t, s; $E(t)$ = relaxation modulus in the linear

96 viscoelastic stage, MPa; and $\varepsilon(t)$ = measured strain history, $\mu\varepsilon$.

97
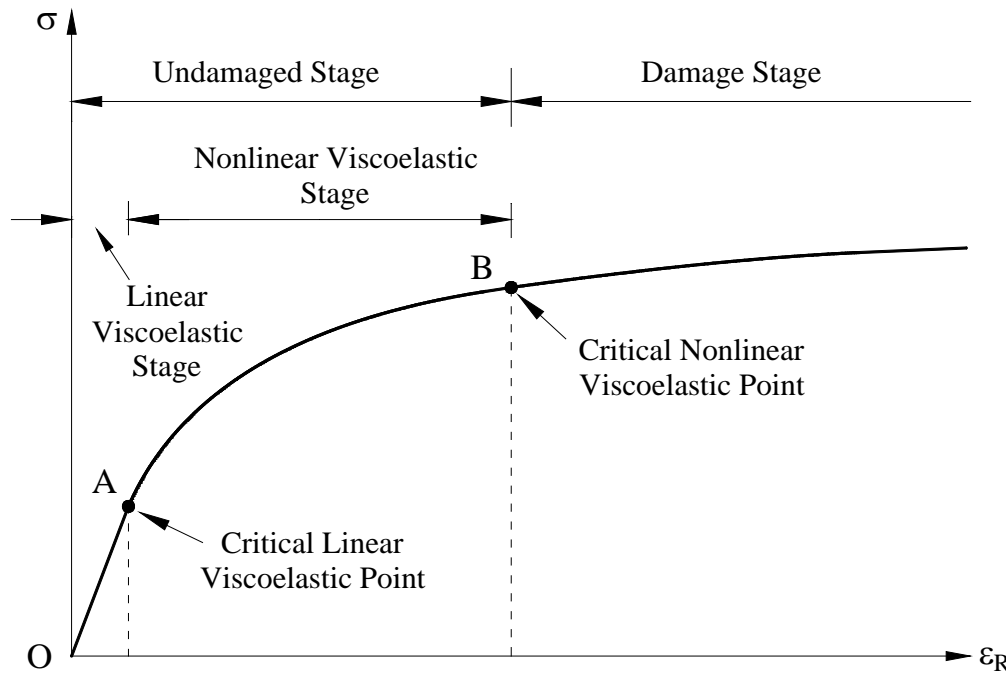
Figure 1 Stress-pseudostrain curve of an asphalt mixture in controlled-strain RDT tests (after [1][2])

Based on the identification of these distinct stages, testing to determine the mechanical properties of asphalt mixtures is made simpler and more precise by using pseudostrain concepts in analyzing the test data. However, these advantages are diminished or even lost if the analysis does not make clear distinctions and boundaries between these stages. In fact, the nonlinear viscoelastic properties are usually muddled up with the linear viscoelastic properties [1][2][4][5]. For example, $\sigma_{VE}(t)$ has been considered to be the same as the measured stress in the nonlinear viscoelastic stage, and E_R has been chosen to be the magnitude of the complex modulus at the critical nonlinear viscoelastic point (Point B) shown in Figure 1 when calculating the pseudostrain in the nonlinear viscoelastic stage [1][2]. These confusions directly lead to the incorrect determination of the pseudostrains and pseudostrain energies in the nonlinear viscoelastic stage and in the damage stage. Using these incorrectly determined results could hardly make accurate prediction of the development of the damages in the asphalt mixture, such as the fatigue cracking and permanent deformation, which are driven by the corresponding dissipated pseudostrain energies (DPSEs). As a result, there is an urgent need to rigorously determine the nonlinear viscoelastic properties of the asphalt mixture in typical controlled-strain RDT tests and to characterize the associated DPSEs in the nonlinear viscoelastic stage and damage stage.

119   To address this research need, this study employed a Dynamic Mechanical Analyzer

120   (DMA) to perform controlled-strain RDT tests on fine aggregate mixture (FAM) specimens

121   in order to investigate their material properties in the linear viscoelastic stage, nonlinear

122   viscoelastic stage and damage stage. The DPSEs in these stages were also characterized for

123   future applications to the prediction of the damage development in asphalt mixtures. The next

124   section describes the configuration and procedure of the controlled-strain RDT tests. The

125   subsequent section presents the determination of the asphalt mixture properties in different

126   stages based on the test data. The following section details the differentiation and

127   characterization of the linear viscoelastic stage, nonlinear viscoelastic stage and damage stage

128   in terms of the viscoelastic stress, pseudostrain and DPSE. The final section summarizes the

129   major findings of this study and briefs the authors' ongoing research on this subject.

130

131   **2.   Configuration and procedure of the controlled-strain RDT tests**

132   *2.1.   Specimen fabrication*

133   FAM specimens for the controlled-strain RDT tests were fabricated in the laboratory

134   using an unmodified #70 petroleum asphalt binder (graded based on the penetration) and fine

135   limestone aggregates passing No. 16 sieve with the opening of 1.18 mm. The gradation of the

136   fine aggregates is listed in Table 1. The asphalt binder content was calculated to be 8.97% by

137   weight of aggregates using the aggregate surface area method with the optimum asphalt

138   content of the corresponding full asphalt mixture [6]–[9].

139

140   **Table 1 Gradation of the fine aggregates in FAM specimens**

Sieve No.	No. 16	No. 30	No. 50	No. 200	PAN (-No. 200)
Sieve Size (mm)	1.18	0.60	0.30	0.75	<0.075
Individual Retaining (%)	0	44.23	23.46	18.85	13.46

141

142   The procedure of fabricating and preparing the FAM specimens for testing was

143   composed of five major steps as follows:

144   (1) Mixing and compaction: the aggregate batch was mixed with the asphalt binder at

145   the temperature of 135°C; after being cured at 121°C for 2 hours, the asphalt

146   mixture was compacted using the Superpave Gyratory Compactor (SGC) into a

147   cylindrical raw specimen 150 mm in diameter and 70 mm in height, as shown in

148   Figure 2(a);

149   (2) Cutting: the upper and lower part of the raw specimen were cut off using an

150   automatic saw into a shorter specimen 40 mm in height, as presented in Figure

151   2(b);

152   (3) Coring: the shorter specimen were cored following the pattern illustrated using red

153   circles in Figure 2(c) to obtain cylindrical specimens to be tested, which were 12

154   mm in diameter and 40 mm in height; Figure 2(d) shows an example of the FAM

155   specimen;

156   (4) Gluing: each end of a FAM specimen was glued to an end platen using a 2 ton

157   epoxy with the aid of a specially designed gluing jig, as presented in Figure 2(e),

158   to assure the vertical pedestals of the two end platens were aligned; Figure 2(f)

159   presents an example of the test specimen glued to end platens; and

160   (5) Curing: all specimens with end platens were cured in an environmental chamber at

161   the temperature of 20°C for at least 1 hour to achieve the temperature equilibrium;

162   the specimens were therefore ready for testing.

163

(a) Raw specimen   **(b) Shorter specimen after cutting**

(c) Making cores

(d) FAM specimen

(e) Gluing jig

(f) Glued specimen for testing

164 **Figure 2 Procedure of fabricating and preparing FAM specimens for testing**

165

166 *2.2. Test configuration*

167   The controlled-strain RDT tests were performed on the FAM specimens using the

168 DMA, as shown in Figure 3. Before the test, the test specimen with end platens was mounted

169 on the upper and lower tension fixtures that were attached to the DMA (see Figure 4). As the

170 specimen was in place, the environmental chamber was closed, which was able to control the

171 test temperature in a range from −60°C to 600°C. The test temperature in this study was 20°C.

172 The test protocol was programmed in the software TRIOS designed specifically for the DMA.

173

174

175 **Figure 3 Overview of Dynamic Mechanical Analyzer (DMA)**
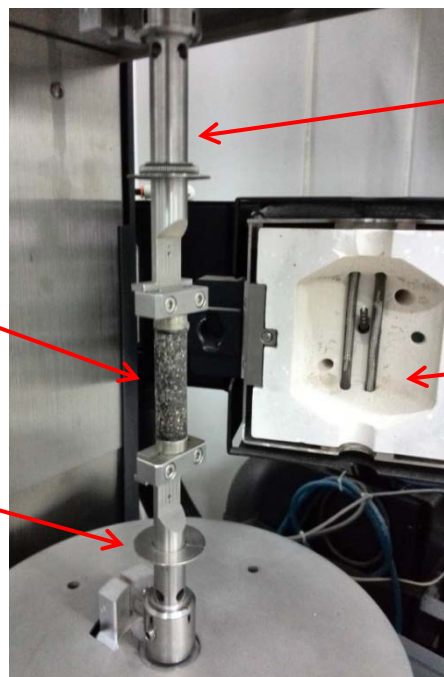
176

177

178 **Figure 4 Configuration of DMA tests**

179

180 *2.3. Test procedure*

181   The entire test procedure consisted of a sequence of consecutive controlled-strain

182 RDT tests at different strain levels, as illustrated in Figure 5. A haversine strain curve was

183 imposed on the specimen in each RDT test, which had 600 loading cycles with a loading

184 frequency of 2π rad/s (1 Hz). There was a 900 s (15 min) rest period between two adjacent

185 RDT tests in order to recover possible deformation in the previous RDT test [1][2].

186
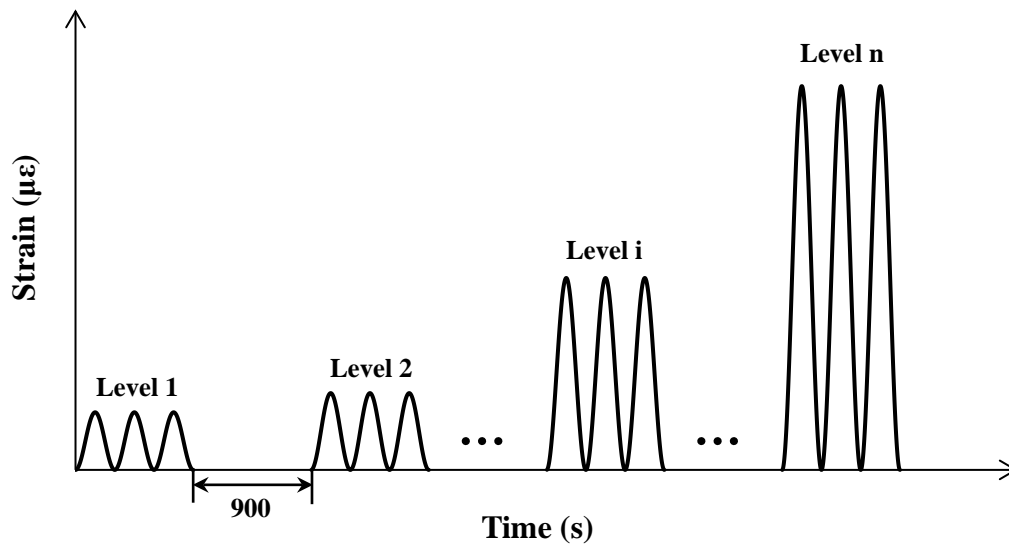
187

188 **Figure 5 Controlled-strain RDT test protocol**

189

190   The test protocol was designed as follows:

191   (1) First RDT test: the initial strain level (Level 1) of the first RDT test was selected

192   to be 20 με to assure that the specimen was within the linear viscoelastic stage;

193   (2) Subsequent RDT tests from Strain Level 2 to $(n-1)$: the axial strain level was

194   increased with an increment of 10 με until the specimen developed into the

195   damage stage; Strain Level $(n-2)$ corresponded to the critical nonlinear

196   viscoelastic point; and

197   (3) Final RDT test: the final strain level (Level n) was chosen to be 200 με for the

198   purpose of introducing sufficient damages to the specimen.

199

200 **3. Properties of test specimens in three stages**

201   The strain and stress data measured from each RDT test were firstly processed in the

202 software MATLAB using the Fourier series to filter possible noise [10]. The strain amplitude
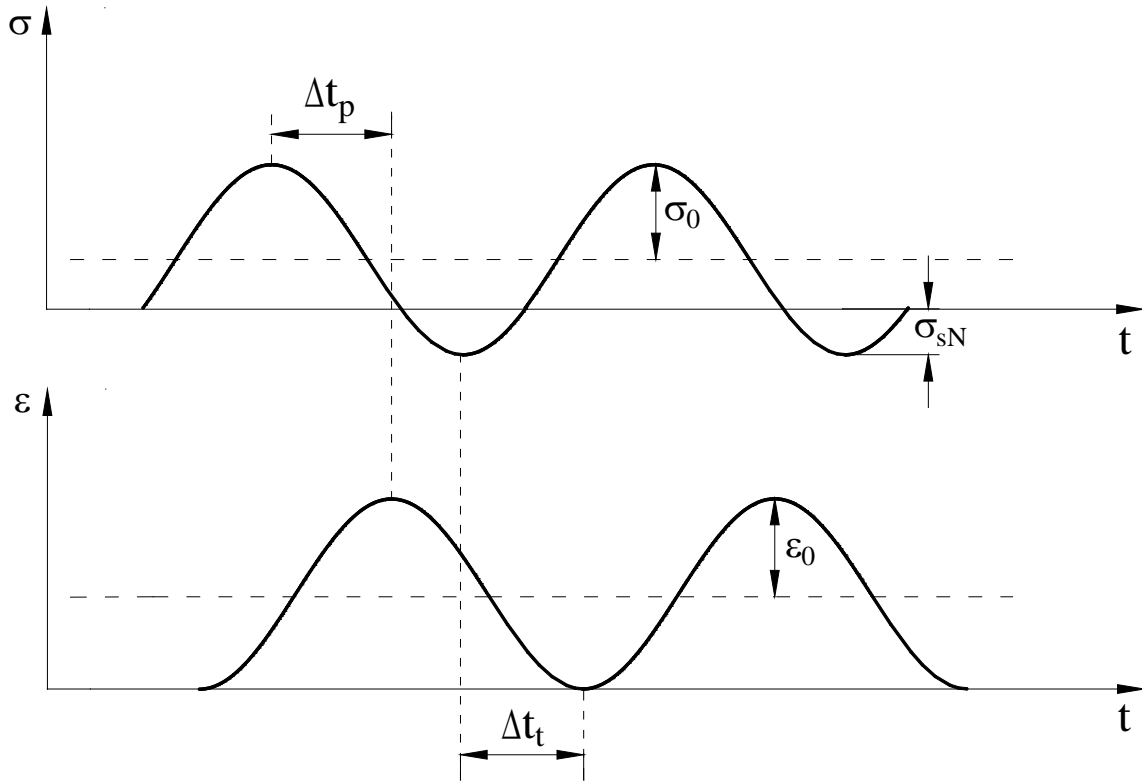
203 (ε_0) and stress amplitude (σ_0) of every loading cycle were therefore determined based on the

204 peaks and troughs of the strain wave and stress wave, respectively, as illustrated in Figure 6.

205 The magnitude of the complex modulus, $\left|E^*\right|$, of every cycle was then calculated to be:

206     $$\left|E^*\right| = \frac{\sigma_0}{\varepsilon_0}$$ (2)

207

8

208

**Figure 6 Stress and strain waves**

210

211   To determine the phase angle of the complex modulus, φ, the time lag between the

212 peaks and the time lag between the troughs of the strain and stress waves in the same loading

213 cycle were identified to be Δt_p and Δt_t, respectively, as shown in Figure 6. It was found that

214 Δt_p and Δt_t were not exactly the same in most loading cycles. Therefore, the average value

215 of Δt_p and Δt_t was used to compute the phase angle of the complex modulus in the

216 corresponding loading cycle as shown in Equation 3:

217
$$\varphi = \frac{\Delta t_p + \Delta t_t}{2} \cdot \omega \tag{3}$$

218 where ω = loading frequency, 2π rad/s. Examples of the determined $\left| E^* \right|$ and φ at strain

219 levels of 30 με, 50 με, 70 με and 200 με are presented in Figure 7, in which φ is converted

220 into degrees for the convenience of visual comparison.

221
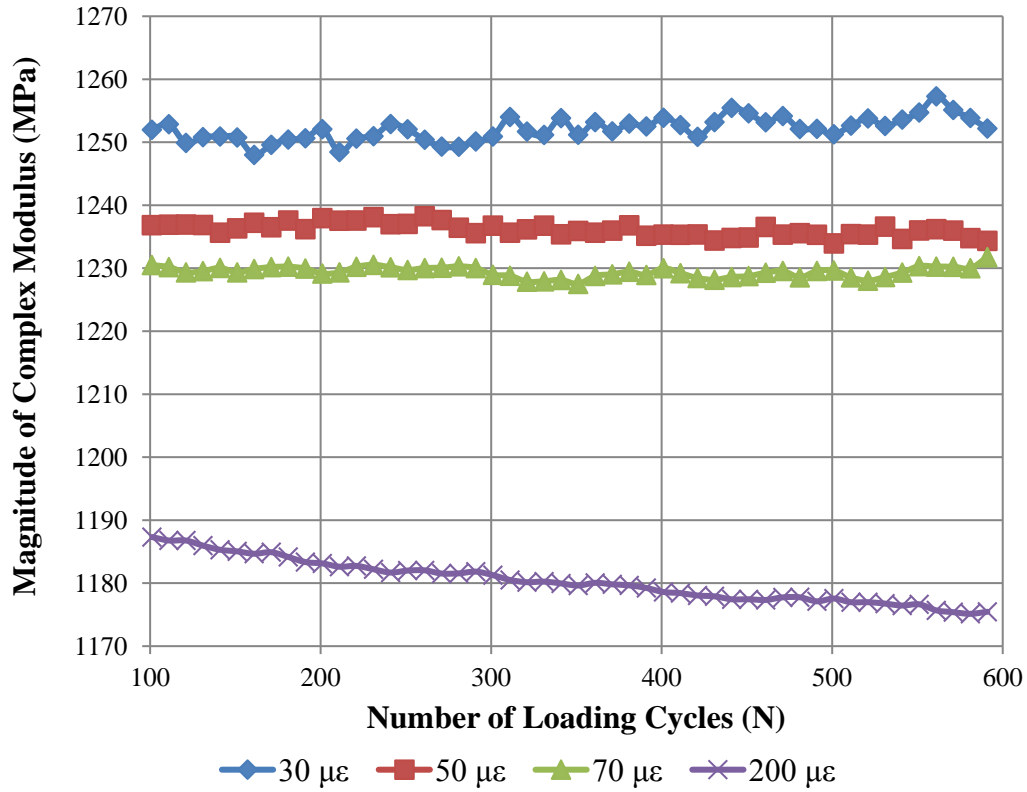
(a) Magnitude of complex modulus
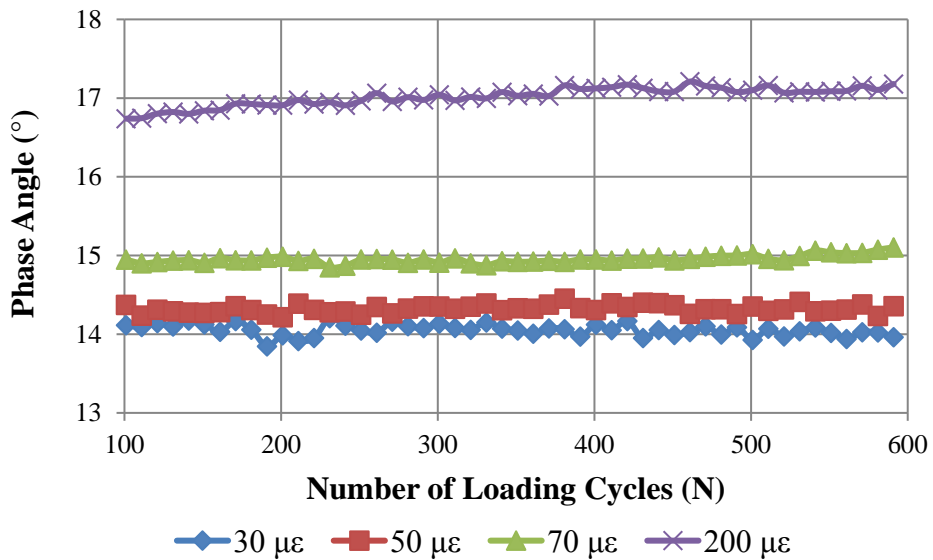
(b) Phase angle of complex modulus

Figure 7 Examples of determined magnitudes and phase angles of complex moduli

The above data analysis was applied to each RDT test starting from Strain Level 1 that was 20 με. The $\left|E^*\right|$ and φ of every loading cycle in each RDT test were therefore

231 determined. According to their characteristics, as detailed in Introduction, the linear

232 viscoelastic stage, nonlinear viscoelastic stage and damage stage were identified for the

233 asphalt mixture specimens tested in this study. It was found that 30 με corresponded to the

234 critical linear viscoelastic point (Point A in Figure 1) and 80 με corresponded to the critical

235 nonlinear viscoelastic point (Point B in Figure 1). Based on the identification of the three

236 stages, the viscoelastic stress, pseudostrain and DPSE will be determined in the next section.

237

238 **4. Characterization of three stages**

239 Based on the measured specimen properties and the identification of the linear

240 viscoelastic, nonlinear viscoelastic and damage stages, these three stages were further

241 characterized and differentiated in terms of the viscoelastic stress, pseudostrain and DPSE.

242 First of all, the pseudostrain was rigorously defined in this study to eliminate the **linear**

243 **viscoelastic** effect only. As a result, regarding the pseudo strain definition shown in Equation

244 1, this study considered $\sigma_{VE}(t)$ to be the linear viscoelastic stress corresponding to the

245 measured strain history, E_R to be the magnitude of the complex modulus in the linear

246 viscoelastic stage and $E(t)$ to be the relaxation modulus in the linear viscoelastic stage. In

247 other words, the material properties in the **linear viscoelastic** stage were the reference

248 properties, based on which the viscoelastic stress, pseudostrain and DPSE were calculated in

249 all three stages as follows.

250

251 *4.1. Viscoelastic stress*

252 To determine the viscoelastic stress, the strain and stress waves measured in each

253 RDT test were firstly simulated using Equations 4 and 5, respectively:

254
$$\varepsilon_m(t) = \varepsilon_0\left[1 - \cos(\omega t - \varphi)\right] = \varepsilon_0 - \varepsilon_0 \cos(\omega t - \varphi) \tag{4}$$

255
$$\sigma_m(t) = \sigma_{0N}\left[1 - \cos(\omega t)\right] - \sigma_{sN} \tag{5}$$

256 where $\varepsilon_m(t)$ = measured strain, με; t = time, s; $\sigma_m(t)$ = measured stress, Pa; σ_{0N} = stress

257 amplitude of the Nth loading cycle, Pa; σ_{sN} = absolute value of the downward shift of the

258 stress curve in the Nth loading cycle, Pa. Equation 4 was then re-arranged as [2]:

259
$$\varepsilon_m(t) = \varepsilon_1(t) - \varepsilon_2(t) \tag{6}$$

260 where $\varepsilon_1(t) = \varepsilon_0$, which was a constant strain history, με; and $\varepsilon_2(t) = \varepsilon_0 \cos(\omega t - \varphi)$, which

261 was a sinusoidal strain history, με.

262   The viscoelastic stresses corresponding to $\varepsilon_1(t)$ and $\varepsilon_2(t)$ were determined to be:

263    $$\sigma_{VE1}(t) = \varepsilon_1(t)E(t) = \varepsilon_0 E(t) \tag{7}$$

264    $$\sigma_{VE2}(t) = \varepsilon_0 \left|E^*\right|_{LVE} \cos(\omega t - \varphi + \varphi_{LVE}) \qquad \text{(Derivation detailed in Appendix)} \tag{8}$$

265   where $\sigma_{VE1}(t)$ = viscoelastic stress corresponding to $\varepsilon_1(t)$, Pa; $E(t)$ = relaxation modulus

266   in the linear viscoelastic stage, MPa; $\sigma_{VE2}(t)$ = viscoelastic stress corresponding to $\varepsilon_2(t)$, Pa;

267    $\left|E^*\right|_{LVE}$ = magnitude of the complex modulus in the linear viscoelastic stage, MPa; φ_{LVE} =

268   phase angle of the complex modulus in the linear viscoelastic stage, rad. Therefore, the

269   viscoelastic stress corresponding to $\varepsilon_m(t)$ was the difference between $\sigma_{VE1}(t)$ and $\sigma_{VE2}(t)$:

270    $$\sigma_{VE}(t) = \varepsilon_0 E(t) - \varepsilon_0 \left|E^*\right|_{LVE} \cos(\omega t - \varphi + \varphi_{LVE}) \tag{9}$$

271   According to the general formulation of $\sigma_{VE}(t)$ presented in Equation 9, specific

272   formulations of $\sigma_{VE}(t)$ were established for the linear viscoelastic, nonlinear viscoelastic and

273   damage stages, respectively:

274   (1) Linear viscoelastic stage: since φ was equal to φ_{LVE}, $\sigma_{VE}(t)$ was simplified as:

275    $$\sigma_{VE}(t) = \varepsilon_0 E(t) - \varepsilon_0 \left|E^*\right|_{LVE} \cos(\omega t) \tag{10}$$

276   (2) Nonlinear viscoelastic stage: at a specific strain level where the phase angle was

277   φ_{NL}, $\sigma_{VE}(t)$ was formulated as:

278    $$\sigma_{VE}(t) = \varepsilon_0 E(t) - \varepsilon_0 \left|E^*\right|_{LVE} \cos(\omega t - \varphi_{NL} + \varphi_{LVE}) \tag{11}$$

279   (3) Damage stage: the formulation of $\sigma_{VE}(t)$ in a specific loading cycle with a phase

280   angle of φ_D was developed as:

281    $$\sigma_{VE}(t) = \varepsilon_0 E(t) - \varepsilon_0 \left|E^*\right|_{LVE} \cos(\omega t - \varphi_D + \varphi_{LVE}) \tag{12}$$

282   The above formulations of $\sigma_{VE}(t)$ will be used to determine the pseudostrain and DPSE in

283   the following subsections.

284

285   *4.2. Pseudostrain*

286   To calculate the pseudostrains in all three stages, $E(t)$ was further derived based on

287   the formulation of $\sigma_{VE}(t)$ in the viscoelastic stage. Since $\sigma_{VE}(t)$ and $\sigma_m(t)$ were exactly the

288 same in the linear viscoelastic stage, Equation 13 was firstly established for the linear

289 viscoelastic stage:

290 $$\sigma_{VE}(t) = \sigma_m(t) \tag{13}$$

291 According to Equation 13, $E(t)$ was then derived based on Equations 5 and 10:

292 $$E(t) = \left|E^*\right|_{LVE} - \frac{\sigma_{s,LVE}(t)}{\varepsilon_{0,LVE}} \tag{14}$$

293 where $\sigma_{s,LVE}(t)$ = absolute value of the downward shift of the stress curve in an RDT test in

294 the linear viscoelastic stage, Pa; $\varepsilon_{0,LVE}$ = strain amplitude of the same RDT test, με. For a

295 specific loading cycle in any RDT test, both $E(t)$ and $\sigma_{s,LVE}(t)$ were considered to be

296 constants within the loading cycle. As a result, the value of $E(t)$ in the Nth loading cycle of a

297 specific RDT test in the linear viscoelastic stage was determined to be:

298 $$E_N = \left|E^*\right|_{LVE} - \frac{\sigma_{sN,LVE}}{\varepsilon_{0,LVE}} \tag{15}$$

299 where E_N = the value of the relaxation modulus in the Nth loading cycle of an RDT test in the

300 linear viscoelastic stage, MPa; and $\sigma_{sN,LVE}$ = absolute value of the downward shift of the

301 stress curve in the Nth loading cycle of the same RDT test, Pa.

302 Based on the determination of the relaxation modulus, the pseudostrains in the three

303 stages were determined using Equation 1 with the terms defined at the beginning of this

304 section, which are detailed as follows.
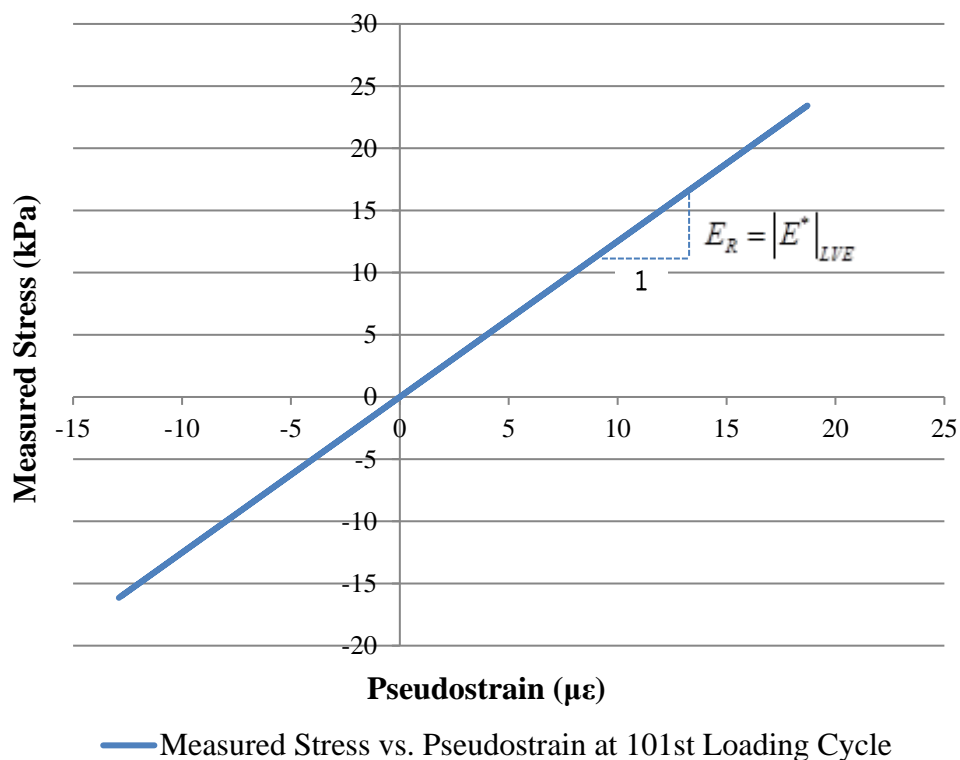
305 (1) Linear viscoelastic stage

306 The pseudostrain was calculated based on Equations 1, 10 and 14:

307
$$\begin{aligned}
\varepsilon_R(t) &= \frac{\sigma_{VE}(t)}{E_R} \\
&= \frac{\varepsilon_0 E(t) - \varepsilon_0 \left|E^*\right|_{LVE} \cos(\omega t)}{\left|E^*\right|_{LVE}} \\
&= \frac{\varepsilon_0 \left(\left|E^*\right|_{LVE} - \dfrac{\sigma_{s,LVE}(t)}{\varepsilon_{0,LVE}}\right) - \varepsilon_0 \left|E^*\right|_{LVE} \cos(\omega t)}{\left|E^*\right|_{LVE}}
\end{aligned} \tag{16}$$

308 Since $\varepsilon_0 = \varepsilon_{0,LVE}$ for a specific RDT test in the linear viscoelastic stage, Equation 17 was then

309 established for the Nth loading cycle of the RDT test:

310
$$\varepsilon_{RN}(t) = \varepsilon_0 \left[1 - \cos(\omega t)\right] - \frac{\sigma_{sN,LVE}}{\left|E^*\right|_{LVE}}$$
(17)

311   Comparing Equations 5 to 17 showed that $\varepsilon_R(t)$ was in phase with $\sigma_m(t)$. As a

312   result, if plotting the measured stress versus pseudostrain, it became a straight line instead of

313   a hysteresis loop, and this straight line passed through the origin. Figure 8 presents an

314   example of the $\sigma_m(t)$ vs. $\varepsilon_R(t)$ graph of the 101st loading cycle of the RDT test with a strain

315   level of 30 με. This graph demonstrated that the entire linear viscoelastic effect was

316   successfully removed in the linear viscoelastic stage, which validated the pseudostrain

317   formulation established in this study.

318

Measured Stress vs. Pseudostrain at 101st Loading Cycle

319
320   **Figure 8 Measured stress vs. pseudostrain in the linear viscoelastic stage**
321   **(Strain level = 30 με)**
322

323   (2) Nonlinear viscoelastic stage

324   The pseudostrain in the nonlinear viscoelastic stage was determined based on

325   Equations 1, 11 and 14:

$$\varepsilon_R\left(t\right)=\frac{\sigma_{VE}\left(t\right)}{E_R}$$

$$=\frac{\varepsilon_0 E\left(t\right)-\varepsilon_0\left|E^*\right|_{LVE}\cos\left(\omega t-\varphi_{NL}+\varphi_{LVE}\right)}{\left|E^*\right|_{LVE}}$$

$$=\frac{\varepsilon_0\left(\left|E^*\right|_{LVE}-\frac{\sigma_{s,LVE}\left(t\right)}{\varepsilon_{0,LVE}}\right)-\varepsilon_0\left|E^*\right|_{LVE}\cos\left(\omega t-\varphi_{NL}+\varphi_{LVE}\right)}{\left|E^*\right|_{LVE}}$$

$$=\varepsilon_0\left[1-\cos\left(\omega t-\varphi_{NL}+\varphi_{LVE}\right)\right]-\frac{\varepsilon_0}{\varepsilon_{0,LVE}}\cdot\frac{\sigma_{s,LVE}\left(t\right)}{\left|E^*\right|_{LVE}}$$

(18)

327 The pseudostrain formulation for the Nth loading cycle of an RDT test in the nonlinear

328 viscoelastic stage was then derived as:

329
$$\varepsilon_{RN}\left(t\right)=\varepsilon_0\left[1-\cos\left(\omega t-\varphi_{NL}+\varphi_{LVE}\right)\right]-\frac{\varepsilon_0}{\varepsilon_{0,LVE}}\cdot\frac{\sigma_{sN,LVE}}{\left|E^*\right|_{LVE}}$$
(19)

330 Comparing Equations 5 to 19 indicated that $\varepsilon_R\left(t\right)$ was no longer in phase with $\sigma_m\left(t\right)$.

331 The phase angle between $\varepsilon_R\left(t\right)$ and $\sigma_m\left(t\right)$ was $\left(\varphi_{NL}-\varphi_{LVE}\right)$, which was larger than zero

332 since $\varphi_{NL}>\varphi_{LVE}$. In a specific RDT test in the nonlinear viscoelastic stage, $\left(\varphi_{NL}-\varphi_{LVE}\right)$

333 stayed unchanged as the number of loading cycles increased because of the characteristics of

334 this stage as stated in previous sections. The $\sigma_m\left(t\right)$ vs. $\varepsilon_R\left(t\right)$ graph of any loading cycle

335 exhibited an ellipse-shaped hysteresis loop, whose center was not located at the origin. The

336 area of this ellipse was the DPSE spent overcoming the sole effect of the nonlinear

337 viscoelasticity since the entire linear viscoelastic effect was eliminated already with the aid of

338 the pseudostrain formulation. Figure 9 presents an example of the $\sigma_m\left(t\right)$ vs. $\varepsilon_R\left(t\right)$ graph at

339 the 101st loading cycle of the RDT test with a strain level of 80 με in the nonlinear

340 viscoelastic stage.

341

Measured Stress vs. Pseudostrain at 101st Loading Cycle
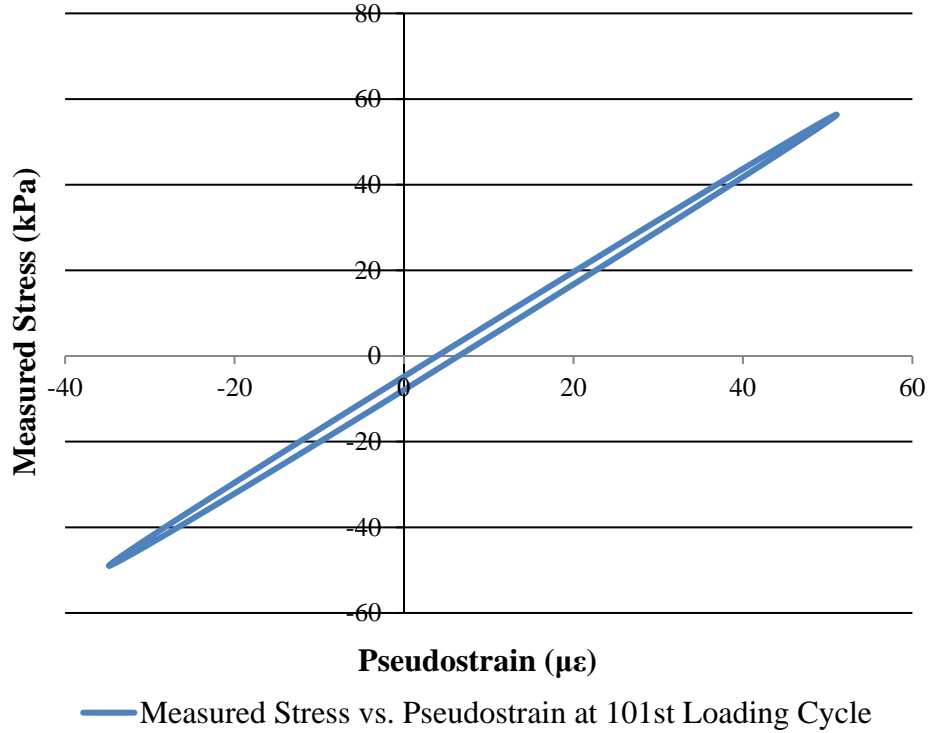
Figure 9 Measured stress vs. pseudostrain in the nonlinear viscoelastic stage

(Strain level = 80 με)

(3) <u>Damage stage</u>

The pseudostrain in the damage stage was formulated based on Equations 1, 12 and 14:

$$
\begin{aligned}
\varepsilon_R(t) &= \frac{\sigma_{VE}(t)}{E_R} \\
&= \frac{\varepsilon_0 E(t) - \varepsilon_0 \left|E^*\right|_{LVE} \cos\left(\omega t - \varphi_D + \varphi_{LVE}\right)}{\left|E^*\right|_{LVE}} \\
&= \frac{\varepsilon_0 \left(\left|E^*\right|_{LVE} - \dfrac{\sigma_{s,LVE}(t)}{\varepsilon_{0,LVE}}\right) - \varepsilon_0 \left|E^*\right|_{LVE} \cos\left(\omega t - \varphi_D + \varphi_{LVE}\right)}{\left|E^*\right|_{LVE}} \\
&= \varepsilon_0 \left[1 - \cos\left(\omega t - \varphi_D + \varphi_{LVE}\right)\right] - \frac{\varepsilon_0}{\varepsilon_{0,LVE}} \cdot \frac{\sigma_{s,LVE}(t)}{\left|E^*\right|_{LVE}}
\end{aligned}
\tag{20}
$$

For the Nth loading cycle of an RDT test in the damage stage, the pseudostrain was formulated as:

$$
\varepsilon_{RN}(t) = \varepsilon_0 \left[1 - \cos\left(\omega t - \varphi_D + \varphi_{LVE}\right)\right] - \frac{\varepsilon_0}{\varepsilon_{0,LVE}} \cdot \frac{\sigma_{sN,LVE}}{\left|E^*\right|_{LVE}}
\tag{21}
$$

16

353   When comparing Equation 5 to Equation 21, it was obviously concluded that $\varepsilon_R(t)$

354   was out of phase with $\sigma_m(t)$ in the damage stage. The phase angle was $(\varphi_D - \varphi_{LVE})$, which

355   was increasing as the number of loading cycles increased in the destructive RDT test. The

356    $\sigma_m(t)$ vs. $\varepsilon_R(t)$ hysteresis loop of any loading cycle also exhibited an ellipse, whose center

357   was not located at the origin either. The area of this ellipse was the DPSE spent for the

358   following purposes:

359   • Overcoming the nonlinear viscoelastic effect; and

360   • Developing damages such as cracking and permanent deformation.

361   Figure 10 shows the $\sigma_m(t)$ vs. $\varepsilon_R(t)$ graph of the 101st loading cycle of the RDT test with a

362   strain level of 200 με in the damage stage.

363
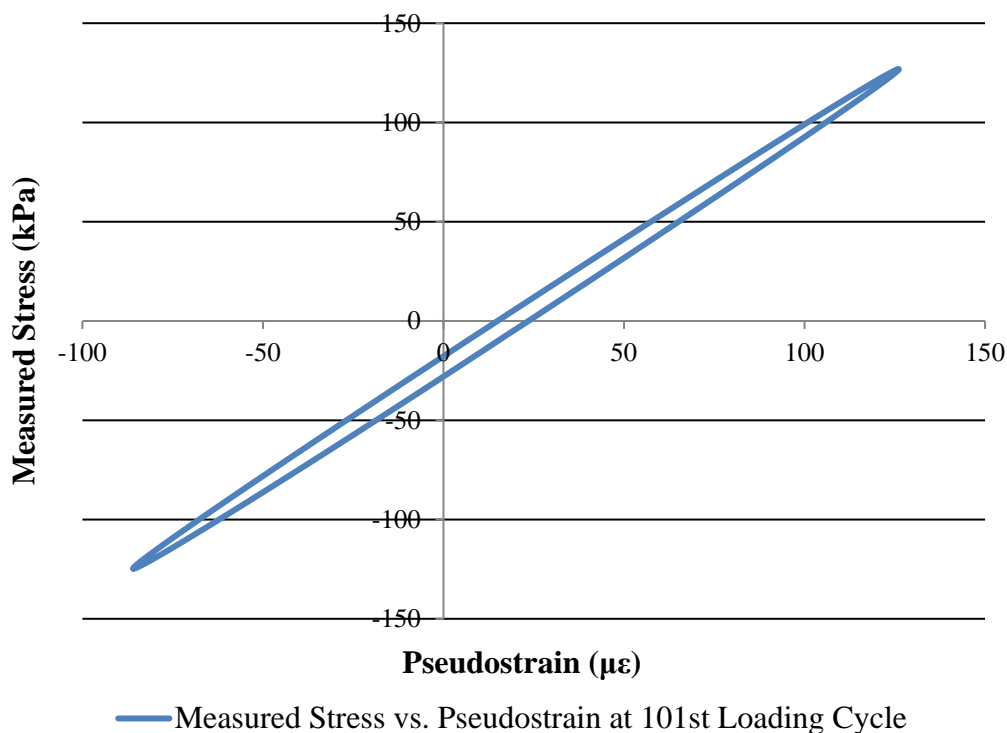
Figure 10 Measured stress vs. pseudostrain in the damage stage

(Strain level = 200 με)

367

368   *4.3. Dissipated pseudostrain energy (DPSE)*

369   As previously explained, the value of the DPSE was the area of the $\sigma_m(t)$ vs. $\varepsilon_R(t)$

370   hysteresis loop. The mathematical formulation of the DPSE was shown in Equation 22 [1][2]

371   [11][12]:

372
$$DPSE = \int_{t_1}^{t_2} \sigma_m(t) \frac{\partial \varepsilon_R(t)}{\partial t} dt \tag{22}$$

373 Based on Equation 22, the DPSEs of representative loading cycles in the linear viscoelastic,

374 nonlinear viscoelastic and damage stages were determined, respectively.

375   (1) Linear viscoelastic stage

376   Since the $\sigma_m(t)$ vs. $\varepsilon_R(t)$ hysteresis loop was in fact a straight line, the DPSE in a

377 loading cycle of any RDT test in the linear viscoelastic stage was equal to zero. This fact

378 indicated that there was no DPSE spent overcoming the linear viscoelastic effect.

379   (2) Nonlinear viscoelastic stage

380   For any loading cycle in the nonlinear viscoelastic stage, the terms of the integrand in

381 Equation 22, $\sigma_m(t)$ and $\varepsilon_R(t)$, were presented in Equations 5 and 19, respectively.

382 Therefore, the DPSE of a loading cycle in this stage was calculated to be:

383
$$DPSE = \int_{t_0}^{t_0+\frac{2\pi}{\omega}} \left\{ \sigma_{0N}\left[1-\cos(\omega t)\right] - \sigma_{sN} \right\} \frac{\partial\left\{ \varepsilon_0\left[1-\cos(\omega t - \varphi_{NL}+\varphi_{LVE})\right] - \frac{\varepsilon_0}{\varepsilon_{0,LVE}} \cdot \frac{\sigma_{sN,LVE}}{|E^*|_{LVE}} \right\}}{\partial t} dt$$

384 $$\tag{23}$$

385 Since $\omega = 2\pi$ rad/s, Equation 23 was simplified to be:

386
$$DPSE = \pi\sigma_{0N}\varepsilon_0 \sin(\varphi_{NL} - \varphi_{LVE}) \tag{24}$$

387   (3) Damage stage

388   When calculating the DPSE in a complete loading cycle in the damage stage, the

389 formulations of $\sigma_m(t)$ and $\varepsilon_R(t)$ in the integrand in Equation 22 were presented in

390 Equations 5 and 21, respectively. Consequently, the DPSE in a loading cycle in the damage

391 stage was formulated as:

392
$$DPSE = \int_{t_0}^{t_0+\frac{2\pi}{\omega}} \left\{ \sigma_{0N}\left[1-\cos(\omega t)\right] - \sigma_{sN} \right\} \frac{\partial\left\{ \varepsilon_0\left[1-\cos(\omega t - \varphi_{D}+\varphi_{LVE})\right] - \frac{\varepsilon_0}{\varepsilon_{0,LVE}} \cdot \frac{\sigma_{sN,LVE}}{|E^*|_{LVE}} \right\}}{\partial t} dt$$

393 $$\tag{25}$$

394 The definite integral was calculated to be:

395
$$DPSE = \pi\sigma_{0N}\varepsilon_0 \sin(\varphi_{D} - \varphi_{LVE}) \tag{26}$$

396   Using Equations 24 and 26, the DPSE of every loading cycle was determined for each

397 RDT test in the nonlinear viscoelastic stage and the damage stage. The determined DPSEs of

398 selected loading cycles in the RDT tests with different strain levels in the nonlinear

18

399   viscoelastic stage are presented in Figure 11, which demonstrates the following

400   characteristics:

401   (1) The DPSEs of all loading cycles stayed approximately constant as the number of

402   loading cycles increased; and

403   (2) When the strain level increased to a higher level within this stage, the DPSE of the

404   loading cycle increased to a larger value.

405   Figure 12 exhibits the determined DPSEs of loading cycles in the RDT test with a

406   strain level of 200 $\mu\varepsilon$, which is in the damage stage. It is clearly illustrated that the DPSE had

407   sustained growth while the number of loading cycles was increasing. This fact indicated that,

408   with the increasing number of loading cycles, an increasing amount of DPSE accumulated to

409   drive the development of damages such as cracking and permanent deformation in the asphalt
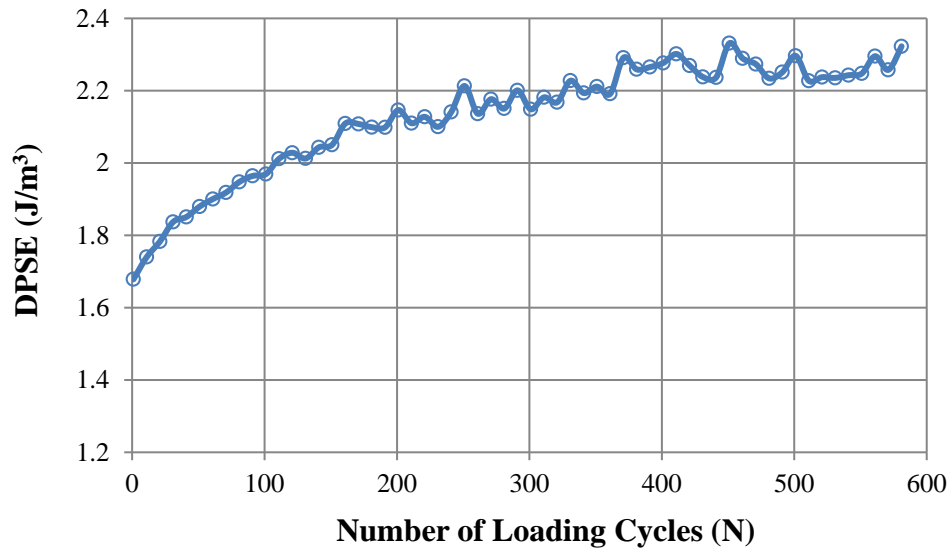
410   mixture specimen.

411
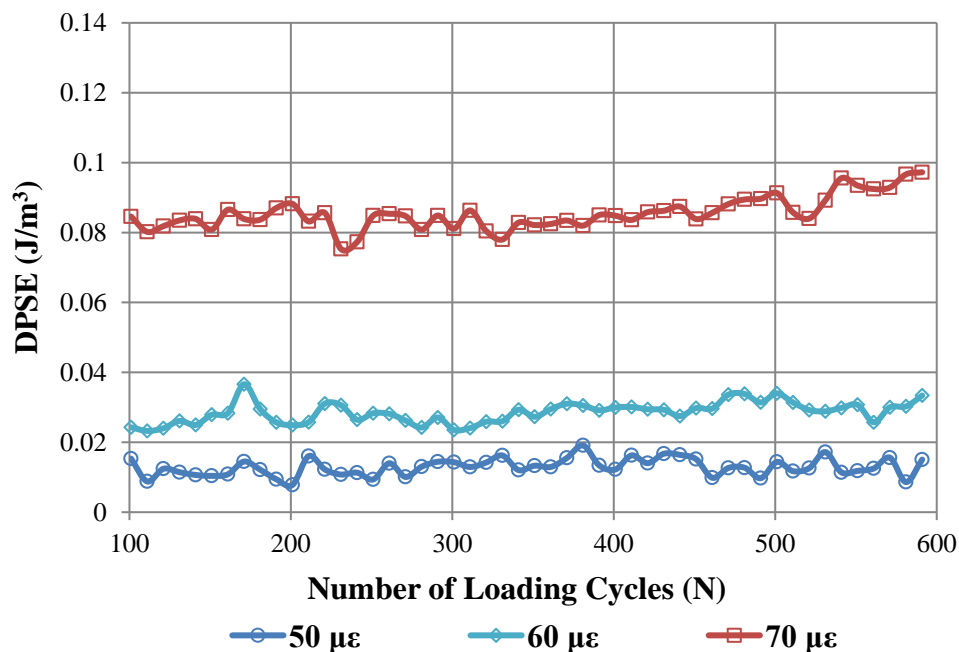
413   **Figure 11 DPSE of loading cycles in RDT tests in nonlinear viscoelastic stage**

414   **(Strain level = 50, 60, 70 $\mu\varepsilon$)**

415

Figure 12 DPSE of loading cycles in an RDT test in damage stage

(Strain level = 200 με)

5. Conclusions

This study investigated the material properties of FAM specimens in the linear viscoelastic stage, nonlinear viscoelastic stage and damage stage. These three stages were differentiated and characterized in terms of the viscoelastic stress, pseudostrain and DPSE based on the measurements of controlled-strain RDT tests at a variety of strain levels, which were performed using the DMA. The definitions of viscoelastic stress, reference modulus and pseudostrain were rigorously established in the analysis in order to assure that the material properties in the linear viscoelastic stage were the reference properties. As a result, only the linear viscoelastic effect was eliminated when determining the pseudostrain and DPSE in the three stages. With the successful elimination of the sole linear viscoelastic effect, the measured stress versus pseudostrain in any loading cycle exhibited a straight line passing through the origin in the linear viscoelastic stage but an ellipse-shaped hysteresis loop, whose center was not located at the origin, in both nonlinear viscoelastic stage and damage stage. The area within the hysteresis loop was the DPSE, which was used for different purposes in the nonlinear viscoelastic stage and damage stage:

    (1) Nonlinear viscoelastic stage: the DPSE was spent in overcoming the nonlinear viscoelastic effect only; and

    (2) Damage stage: the DPSE was spent in overcoming the nonlinear viscoelastic effect and in developing damages such as cracking and permanent deformation in the asphalt mixture.

440   Based on the formulations of the pseudostrain and DPSE, the DPSEs of all loading

441 cycles were determined for every RDT test at each strain level. The following characteristics

442 of the DPSEs were observed in the three stages:

443   (1) Linear viscoelastic stage: the DPSE of any loading cycle was zero;

444   (2) Nonlinear viscoelastic stage:

445   a. As the number of loading cycles increased, the DPSE of each loading

446   cycle remained approximately the same, which indicated that the same

447   amount of energy was spent overcoming the nonlinear viscoelasticity in

448   every cycle;

449   b. When the strain level of the RDT test increased to a higher level within the

450   nonlinear viscoelastic stage, the DPSE of every loading cycle increased to

451   a larger value and stayed unchanged as the number of loading cycles

452   increased; this fact indicated that more energy was spent overcoming the

453   larger nonlinear viscoelasticity at a higher strain level.

454   (3) Damage stage: with the growth of the number of loading cycles, the DPSE of the

455   loading cycle was increasing, which indicated that a larger amount of DPSE was

456   spent developing damages including cracking and permanent deformation in the

457   asphalt mixtures.

458   The findings of this study are capable of strictly differentiating the linear

459 viscoelasticity from the nonlinear viscoelasticity of asphalt mixtures. Therefore, the

460 pseudostrains and the DPSEs of the nonlinear viscoelastic stage and damage stage can be

461 rigorously determined while eliminating the sole linear viscoelastic effect of the asphalt

462 mixtures. This is critical for the accurate determination of the DPSE spent in overcoming the

463 nonlinear viscoelasticity and in developing damages in the asphalt mixtures. The test and

464 analysis methods developed in this study provide clarity, simplicity and accuracy to the

465 characterization of material properties that are used in the design and construction of asphalt

466 pavements. Based on the definitions and formulations established in this study, the DPSE for

467 overcoming the nonlinear viscoelasticity is further distinguished from the DPSE for driving

468 the damage development in an ongoing investigation for the purpose of establishing energy-

469 based models for predicting damage evolution in asphalt mixtures.

470

478   **References**

479   [1]   Luo, X., Luo, R., and Lytton, R. L. (2013). Characterization of fatigue damage in

480   asphalt mixtures using pseudostrain energy. ASCE *Journal of Materials in Civil*

481   *Engineering*, 25(2), 208-218.

482   [2]   Luo, X., Luo, R., and Lytton, R. L. (2013). Energy-based mechanistic approach to

483   characterize crack growth of asphalt mixtures. ASCE *Journal of Materials in Civil*

484   *Engineering*, 25(9), 1198-1208.

485   [3]   Schapery, R. A. (1984). Correspondence principles and a generalized J integral for large

486   deformation and fracture analysis of viscoelastic media. *International Journal of*

487   *Fracture*, 25(3), 195-223.

488   [4]   Si, Z., Little, D. N., and Lytton, R. L. (2002). Characterization of microdamage and

489   healing of asphalt concrete mixtures. ASCE *Journal of Materials in Civil Engineering*,

490   14(6), 461-470.

491   [5]   Masad, E., Castelo Branco, V. T. F., Little, D. N., and Lytton, R. L. (2008). A unified

492   method for the analysis of controlled-strain and controlled-stress fatigue testing.

493   *International Journal of Pavement Engineering*, 9(4), 233-246.

494   [6]   Zollinger, C. J. (2005). Application of surface energy measurements to evaluate

495   moisture susceptibility of asphalt and aggregates. Master of Science, thesis, Texas

496   A&M University.

497   [7]   Masad, E., Castelo Branco, V. T. F., Little, D. N., and Lytton, R. L. (2006). An

498   improved method for the dynamic mechanical analysis of fatigue failure of sand asphalt

499   mixtures. Federal Highway Administration, Texas Transportation Institute, Texas A&M

500   University, FHWA/473630.

501   [8]   Vasconcelos, K. L., Bhasin, A., Little, D. N. and Lytton, R. L. (2010). Experimental

502   measurement of water diffusion through fine aggregate mixtures. ASCE *Journal of*

503   *Materials in Civil Engineering*, 23(4), 445-452.

504   [9]   Tong, Y., Luo, R., and Lytton, R. L. (2015). Moisture and aging damage evaluation of

505   asphalt mixtures using the repeated direct tensional test method. *International Journal*

506   *of Pavement Engineering*, 16(5), 397-410.

507   [10] *MATLAB* [computer software]. Math Works, Natick, MA.

508   [11] Zhang, Y., Luo, R., and Lytton, R. L. (2013). Mechanistic modeling of fracture in

509   asphalt mixtures under compressive loading. ASCE *Journal of Materials in Civil*

510   *Engineering*, 25(9), 1189-1197.

511   [12] Zhang, Y., Luo, R., and Lytton, R. L. (2014). Anisotropic characterization of crack

512   growth in the tertiary flow of asphalt mixtures in compression. ASCE *Journal of*

513   *Engineering Mechanics*, 140(6), 682-694.

514   [13] Ferry, J. D. (1980). *Viscoelastic properties of polymers*, 3rd edition, Wiley, New York,

515   USA.

516   [14] Findley, W. N., Lai, J. S., and Onaran, K. (1989). *Creep and relaxation of nonlinear*

517   *viscoelastic materials: with an introduction to linear viscoelasticity*. Dove Publications,

518   Mineola, New York, USA.

519   [15] Wineman, A.S., and Rajagopal, K. R. (2000). *Mechanical response of polymers:*

520   *Introduction*. Cambridge University Press, Cambridge, UK.

521

522   **Appendix: Derivation of Equation 8**

523   For a sinusoidal strain history $\varepsilon_2(t) = \varepsilon_0 \cos(\omega t - \varphi_m)$, the corresponding viscoelastic

524   stress $\sigma_{VE2}(t)$ is derived as follows.

$$
\begin{aligned}
\sigma_{VE2}(t) &= \int_0^t E(t-\tau) \frac{\partial \varepsilon_2(\tau)}{\partial \tau} d\tau \\
&= \int_0^t E(t-\tau) \frac{\partial \varepsilon_0 \cos(\omega\tau - \varphi)}{\partial \tau} d\tau \\
&= -\varepsilon_0 \omega \int_0^t E(t-\tau) \sin(\omega\tau - \varphi) d\tau
\end{aligned}
\tag{A.1}
$$

525

526   Let $\xi = t - \tau$, then $\tau = t - \xi$, and when $\tau \in [0,t]$, $\xi \in [t,0]$. Equation A.1 is then re-arranged

527   as:

$$
\begin{aligned}
\sigma_{VE2}(t) &= -\varepsilon_0 \omega \int_0^t E(\xi) \sin\big[\omega(t-\xi) - \varphi\big] d(t-\xi) \\
&= \varepsilon_0 \omega \int_t^0 E(\xi) \sin\big[(\omega t - \varphi) - \omega\xi\big] d\xi \\
&= \varepsilon_0 \omega \int_0^t E(\xi) \big[\sin(\omega\xi)\cos(\omega t - \varphi) - \cos(\omega\xi)\sin(\omega t - \varphi)\big] d\xi \\
&= \varepsilon_0 \omega \left[\int_0^t E(\xi)\sin(\omega\xi) d\xi\right]\cos(\omega t - \varphi) - \varepsilon_0 \omega \left[\int_0^t E(\xi)\cos(\omega\xi) d\xi\right]\sin(\omega t - \varphi)
\end{aligned}
\tag{A.2}
$$

528

529   According to the linear viscoelastic theory [13]–[15], the storage modulus $E'(\omega)$ and

530   the loss modulus $E''(\omega)$ of the complex modulus $E^*(\omega)$ can be expressed as follows:

531
$$E'(\omega) = \omega \int_0^t E(\xi)\sin(\omega\xi)d\xi = \left|E^*\right|_{LVE}\cos\varphi_{LVE} \tag{A.3}$$

532
$$E''(\omega) = \omega \int_0^t E(\xi)\cos(\omega\xi)d\xi = \left|E^*\right|_{LVE}\sin\varphi_{LVE} \tag{A.4}$$

533   Therefore, Equation A.2 is further formulated as:

534
$$\begin{aligned}
\sigma_{VE2}(t) &= \varepsilon_0 E'(\omega)\cos(\omega t - \varphi) - \varepsilon_0 E''(\omega)\sin(\omega t - \varphi) \\
&= \varepsilon_0 \left|E^*\right|_{LVE}\cos\varphi_{LVE}\cos(\omega t - \varphi) - \varepsilon_0\left|E^*\right|_{LVE}\sin\varphi_{LVE}\sin(\omega t - \varphi) \\
&= \varepsilon_0\left|E^*\right|_{LVE}\left[\cos\varphi_{LVE}\cos(\omega t - \varphi) - \sin\varphi_{LVE}\sin(\omega t - \varphi)\right] \\
&= \varepsilon_0\left|E^*\right|_{LVE}\cos(\omega t - \varphi + \varphi_{LVE})
\end{aligned} \tag{A.5}$$

535   To summarize, the viscoelastic stress $\sigma_{VE2}(t)$ corresponding to the strain history

536    $\varepsilon_2(t) = \varepsilon_0\cos(\omega t - \varphi_m)$ is determined to be:

537
$$\sigma_{VE2}(t) = \varepsilon_0\left|E^*\right|_{LVE}\cos(\omega t - \varphi + \varphi_{LVE}) \tag{A.6}$$